Effects of elevated temperature on rubber concrete
Fracture properties and mechanism analysis

Wu, Liangqin; Li, Renfeng; Zhu, Zhiyong; Pan, Tanbo; Aydin, Beyazit Bestami; Zhou, Yubao

DOI
10.1016/j.conbuildmat.2025.140263

Publication date
2025

Document Version
Final published version

Published in
Construction and Building Materials

Citation (APA)
Wu, L., Li, R., Zhu, Z., Pan, T., Aydin, B. B., & Zhou, Y. (2025). Effects of elevated temperature on rubber concrete: Fracture properties and mechanism analysis. *Construction and Building Materials*, *466*, Article 140263. https://doi.org/10.1016/j.conbuildmat.2025.140263

Construction and Building Materials 466 (2025) 140263

Contents lists available at ScienceDirect

Construction and Building Materials

journal homepage: www.elsevier.com/locate/conbuildmat

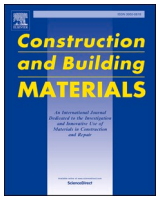

Effects of elevated temperature on rubber concrete: Fracture properties and mechanism analysis

Liangqin Wu [a], Renfeng Li [a], Zhiyong Zhu [a], Tanbo Pan [a,*], Beyazit Bestami Aydin [b], Yubao Zhou [c]

[a] School of Civil Engineering & Architecture, East China Jiaotong University, China
[b] Department of Civil Engineering, Middle East Technical University (METU), Turkey
[c] Faculty of Civil Engineering and Geosciences, Delft University of Technology, the Netherlands

ARTICLE INFO

Keywords:
Rubber concrete
Elevated temperature
Fracture toughness
Fracture process zone (FPZ)
Microstructure evolution

ABSTRACT

Recycling waste tires for the production of concrete materials with good toughness is a green and economical solution, but the severe deterioration of rubber under high temperatures limits its application in engineering practice. Therefore, to examine the impact of elevated temperature on the fracture characteristics of rubber concrete (RC), three-point bending fracture tests were conducted on RC with five rubber replacement rates and five treatment temperatures. The purpose was to correlate the fracture parameters of RC with the rubber replacement rate and the temperature. Then, by employing the digital image correlation (DIC) technology and microscopic testing methods, the crack evolution trend and the potential mechanism were analyzed in detail. The results indicate that rubber particles can effectively improve the toughness, deformation capacity, and fracture energy of concrete, but have a significant weakening effect on the load and fracture performance. When the treatment temperature is below 400 ℃, rubber particles mainly affect the initiation and propagation of cracks by alleviating the stress concentration phenomenon at the crack tip and improving the crack propagation path. Rubber particles may initiate cracks earlier, but significantly delay their propagation process. When the treatment temperature is above 400 ℃, rubber particles tend to exert a weakening effect on the fracture performance. As the temperature rises, the microstructure of rubber particles gradually changes from a relatively uniform state in close contact with the cement matrix to a fragmented state filled with pores separated from the matrix. This process will lead to severe deterioration of concrete performance. It is anticipated that the findings of this study will provide a theoretical basis for predicting the performance of RC in high-temperature environments.

1. Introduction

The rapid development of the automotive industry has brought over a large amount of waste tires, which are a significant burden on the environment. How to recycle waste tires in large scale is nowadays receiving widespread attention [1]. Mixing rubber particles obtained from waste tires into concrete materials has been recognized as a green, eco-friendly, and economically feasible solution [2,3]. It can not only solve the problems of space occupation and environmental pollution, but also improve the deformation and fatigue capacity of concrete by utilizing the advantages of rubber. Therefore, adding rubber particles into concrete is of great environmental and social benefits.

Earlier research has shown that rubber particles, as a kind of flexible filler, can effectively improve the ductility of concrete, although they may reduce the mechanical strength to a certain extent [4–6]. With regard to this situation, a variety of rubber concrete (RC) materials with different properties have been developed to address different engineering requirements. These newly developed RCs usually possess better toughness, cracking resistance, impact resistance, wear resistance, and freeze-thaw cycle performance than ordinary Porland cement (PC) [7–12]. At present, the relevant studies on RC mainly focus on the aspects of rubber replacement rate, particle size, loading method, and mixing of rubber particles with other materials. The main research results indicate that rubber replacement rate and particle size have significant effects on the performance of RC. When the rubber replacement rate is appropriate and the rubber particle size is relatively small, the

* Corresponding author.
E-mail addresses: 2816@ecjtu.edu.cn (L. Wu), 2019211003000212@ecjtu.edu.cn (R. Li), 2022018081406001@ecjtu.edu.cn (Z. Zhu), TanboPan@163.com (T. Pan), b.b.aydin@tudelft.nl (B.B. Aydin), Y.Zhou-16@tudelft.nl (Y. Zhou).

https://doi.org/10.1016/j.conbuildmat.2025.140263
Received 28 November 2024; Received in revised form 27 January 2025; Accepted 30 January 2025
Available online 7 February 2025

toughness and impact resistance of RC can be improved to varying extents. On the other hand, when the rubber replacement rate is too high or the particle size is too large, the mechanical properties of concrete will be greatly weakened while the deformability will be significantly increased, leading to a negative impact on concrete durability.

In modern engineering, fire is an extremely important safety indicator, and potential fire hazards pose a huge threat to buildings and human activities [13,14]. According to existing research, when the temperature reaches 300 ℃, the crystal water in concrete begins to evaporate and the hydration products begin to decompose. When the temperature exceeds 400 ℃, most of the crystal water has been lost, accompanied by the decomposition of $Ca(OH)_2$ [3]. For the rubber material, it has usually completely melted at 200–400 ℃, which is not consistent with the critical temperature of concrete. As a result, RC exhibits different behaviors from PC under different temperatures. Moreover, due to the special composition of concrete itself, there are many initial defects inside the concrete structure after the preparation processes of mixing, vibration, and curing. Under elevated temperature, these defects will be further intensified, making concrete more prone to cracking and leading to deteriorated performance [15,16]. Based on the above analysis, it is of great significance to investigate the initiation and evolution of cracks during the failure process of RC under elevated temperature. To date, there are few studies focusing on this topic. Bengar et al. [17] reported that under high temperatures, the mechanical properties of RC deteriorate more severely with the rise of temperature; specifically, at 800 ℃, the compressive performance of RC containing 20 % rubber particles was reduced by about 85 %. The addition of rubber may weaken the compressive strength of concrete, and this characteristic is further amplified under elevated temperature [17]. In addition, rubber particles tend to soften and decompose at high temperatures; this transition can produce a large amount of gas to hinder the propagation of cracks, but significantly weaken the strength of concrete (the strength of RC is much lower than that of PC) [18–20]. In civil engineering, three-point bending fracture test is an effective method to examine the trends of crack initiation and evolution. This method can directly target the Type I failure mode of cracks for the purpose of analyzing key fracture parameters, which has been validated in recent years [15,21,22]. Studying the fracture properties of RC after high-temperature treatment is of great significance for clarifying the effects of temperature and rubber replacement rate on the initiation and evolution of cracks in concrete. In view of the limited evidence published, carrying out relevant research work has important scientific value.

To clarify the effects of temperature and rubber replacement rate on the fracture properties of concrete and to analyze the corresponding failure mechanism, three-point bending tests were conducted on RC by considering five rubber replacement rates (0 %, 10 %, 20 %, 30 %, and 40 %) and five treatment temperatures (20 ℃, 200 ℃, 400 ℃, 600 ℃, and 800 ℃). Then, by employing the digital image correlation (DIC) and scanning electron microscope (SEM) technology, the fracture failure trend and the underlying mechanism were analyzed in detail. The findings of this study can provide experimental basis and mechanism guidance for predicting the performance deterioration of RC after elevated temperature exposure.

2. Experimental plan

2.1. Raw materials and mix proportions

A key concern of this paper is to study the fracture properties of RC after treatment by different temperatures. The mix proportions of concrete were determined based on the “Specification for mix proportion design of ordinary concrete (JGJ55–2016)” [23] and the previous research [14,24]. The specimens were prepared based on PC with a strength of 30 MPa. The raw materials mainly include: PC (type: P.O 42.5, see Table 1 for specific properties), water (urban tap water), river sand (fineness modulus: 2.5, apparent density: 2650 kg/m^3), coarse aggregates (natural aggregate crushed stone, particle size range: 4 mm~16 mm, apparent density: 2580 kg/m^3), and rubber particles (see Table 2 for specific properties, see Fig. 1 for morphology).

Aiming at the research purpose of this study, five different rubber replacement rates were set for the experiment, namely 0 %, 10 %, 20 %, 30 %, and 40 %. The specimen with a rubber replacement rate of 0 % is actually PC. Specimens with rubber replacement rates of 10 %, 20 %, 30 %, and 40 % were prepared based on PC by replacing fine aggregates with equal volumes of rubber particles. Further, according to the research of Ma et al. [25] and Wang et al. [26] and the actual engineering background, five treatment temperatures were set, namely 20 ℃, 200 ℃, 400 ℃, 600 ℃, and 800 ℃. The specific mix proportions are detailed in Table 3. For the convenience of specimen notation, a specimen with X% rubber replacement rate under the treatment temperature of Y ℃ is denoted as RCX-Y.

2.2. Loading plan

According to the relevant literature [27], the specimen size was determined to be 100 mm× 100 mm× 400 mm. After curing, a 5 mm× 30 mm prefabricated crack was created at the bottom of each specimen (see Fig. 2 for details). To investigate the fracture properties of RC after elevated temperature treatment, a box-type high-temperature furnace was used in this study as the heating equipment. Notably, in order to avoid high-temperature cracking during the heating process, the specimens need to be preprocessed before formal treatment. Referring to Yu et al. [15] and Zhang et al. [26], the specimens were placed in a drying oven (105 ℃) for 72 h first, and then cooled down to room temperature before subjecting for high-temperature treatment (temperature settings: 20 ℃, i.e., room temperature, 200 ℃, 400 ℃, 600 ℃, and 800 ℃). To ensure that the temperature in the center area of each specimen can accurately reach the preset value, a heating rate of 5 ℃/min was adopted, and the temperature was maintained constantly for 2 h after reaching the desired value. Upon the completion of high-temperature treatment, the specimens were taken out from the furnace and cooled down to room temperature properly. To avoid the impact of prolonged standing on the recovery of mechanical properties, the experiment was conducted within 24 h after the specimens returned to room temperature [28]. Based on the specific equipment conditions and previous research [22,29], the displacement control loading method was adopted with a rate of 0.05 mm/min. The loading process was stopped after a specimen was completely destroyed. The load (P) and crack mouth opening displacement (CMOD) data under different test conditions were acquired for further analysis. To obtain the entire crack propagation process, the DIC technology was employed to clarify the damage evolution process, CMOD, and the length of fracture process

Table 1
Physical properties of ordinary Portland cement (P.O 42.5).

Fineness (%)	Initial setting time (min)	Final setting time (min)	Stability	Loss on ignition (%)	Compressive strength (MPa)		Flexural strength (MPa)	
					3d	28d	3d	28d
3.8	125	180	Qualified	2.1	26.3	54.2	5.1	8.2

Table 2
Rubber granules performance indicators.

Density (kg/m^3)	Apparent density (kg/m^3)	Bulk density (kg/m^3)	Tensile strength (MPa)	Water absorption rate (%)	Elongation rate (%)	Fiber content (%)
1330	1270	820	> 15	< 10	> 500	< 0.1 %

Fig. 1. Morphology of rubber particles.

Table 3
RC specimens with different rubber replacement rates (Unit: kg/m^3).

Rubber replacement rate (%)	Cement	Water	Fine aggregates	Rubber particles	Coarse aggregates
0	279	178	780	0	1034
10	279	178	702	32.3	1034
20	279	178	624	64.6	1034
30	279	178	546	96.9	1034
40	279	178	468	129.2	1034

zone under various test conditions. Taking into account the random characteristics of concrete materials and to ensure the accuracy of the test results, the hydraulic servo system and high-speed camera were simultaneously activated during the experiment, and three parallel specimens were tested for each condition.

2.3. Experimental equipment

According to the loading plan described above, the experimental equipment for the three-point bending fracture test mainly includes a high-temperature furnace, a hydraulic servo machine, an extensometer, a high-speed camera, and an SEM device. More specifically, the high-temperature furnace adopted a box-type furnace, with a maximum temperature of 1000 ℃ and a precision of ± 1 ℃, as shown in Fig. 3. The hydraulic servo machine adopted the Wance ETM series microcomputer controlled electronic universal testing machine, with a maximum load of

Fig. 3. High-temperature furnace.

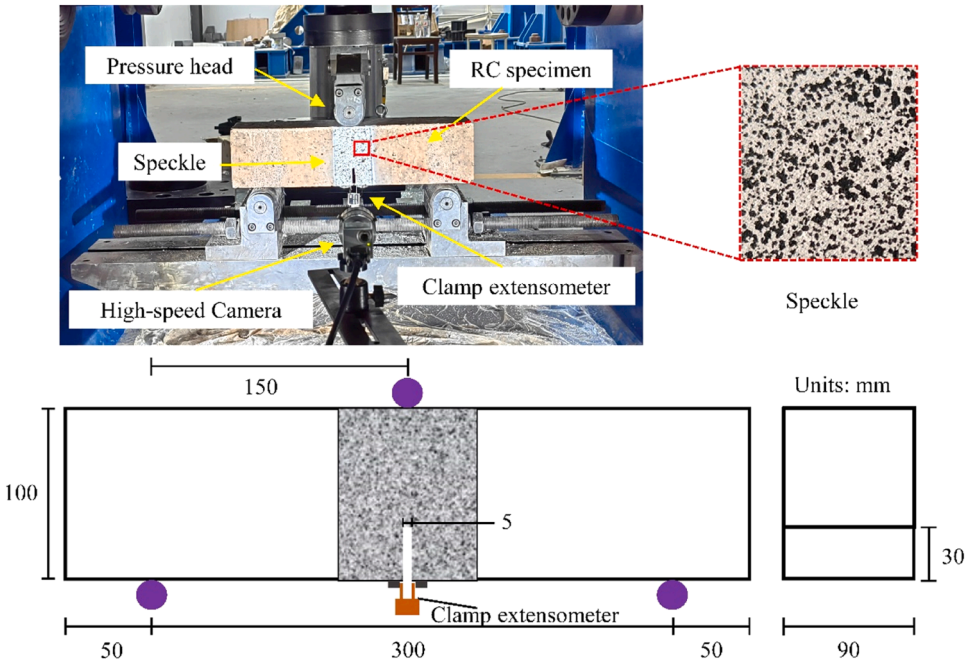

Fig. 2. Specimen size and loading process of three-point bending fracture test.

2000KN and an error range within ± 1 %. The extensometer is a clamp-type extensometer with a maximum measurement range of 10 mm and an error within ± 1 %. The hydraulic servo machine and extensometer are shown in Fig. 2. The high-speed camera used in this study has a resolution of 12.3 M pixels and a maximum frame rate of 120 Hz (the frame rate for this experiment was set to 33 Hz), and is equipped with two LED spotlights to adjust the lighting conditions in order to properly capture the image data of the fracture process (see Fig. 2). The SEM device is a Regulus 8230 HR cold field emission SEM. To ensure sufficient clarity of the test results, a conductive coating was applied to each specimen before testing, and vacuum treatment was performed with the specimen being placed on the specimen stage. The experimental equipment is shown in Fig. 3 and Fig. 4.

3. Results and analysis

3.1. Failure morphology

From the three-point bending tests on RC specimens under different test conditions, the corresponding failure morphology was obtained, as shown in Fig. 5. The marked areas in the figure are typical regions on the interface between rubber particles and the surrounding cement matrix, which can be used to conduct qualitative analysis on the interfacial properties after different temperature treatments.

According to Fig. 5, both the temperature and rubber replacement rate have significant effects on the failure morphology of RC specimens. For PC specimens, there is no significant difference in the failure morphology between 20 ℃ and 200 ℃ test conditions. With the increase of temperature, the color of the failure section gradually deepens, transitioning from dark gray to light red, which is mainly attributed to the presence of iron elements. More specifically, as the temperature increases to a certain level (i.e., above 400 ℃ in this study), iron elements will undergo chemical reactions to generate oxides, causing the color to change towards red. Notably, the red substances were mainly observed around the prefabricated crack, where the iron elements could be exposed to sufficient oxygen. After 600 ℃ and 800 ℃ treatments, the center area of the specimen also exhibits a dark clustering region significantly different from other test conditions. The reason can be explained as follows: after drying pretreatment, a large amount of water in the specimens will evaporate under 20 ℃ and 200 ℃ treatments, but the main hydration products, C-S-H gel and $Ca(OH)_2$, are basically unaffected. Then, as the temperature reaches 400 ℃, both C-S-H gel and $Ca(OH)_2$ begin to decompose, and the degree of decomposition is positively correlated with the temperature and negatively correlated with the distance from the specimen surface. Therefore, the color difference is most obvious on the specimen after 800 ℃ treatment.

The RC specimens also exhibit a red color deepening phenomenon with the rise of temperature, and the color differences are more obvious after 600 ℃ and 800 ℃ treatments compared to PC. This is because rubber particles have a good heat insulation effect, which can weaken the efficiency of internal heat transfer. Thus, compared to PC, RC specimens present with larger dark color areas inside the concrete structure (i.e., more C-S-H gel and $Ca(OH)_2$ are not decomposed). It is worth noting that the marked area in Fig. 5 indicates the bonding area between rubber particles and the cement matrix after high-temperature treatment. It can be found that the degree of bonding between rubber particles and the matrix shows a significant weakening trend with the rise of temperature (see details in Fig. 6). After 20 ℃ treatment, the rubber particles are tightly bound to the matrix, while after 200 ℃ treatment, the degree of binding decreases slightly. After 400 ℃ treatment, significant deterioration has occurred around the rubber particles, and the interface layers around the rubber particles are no longer dense, with pores beginning to appear. After 600 ℃ treatment, microcracks have occurred at the interface layers. As the temperature reaches 800 ℃, the interface layers have basically disappeared, leaving significant cracks, and the rubber particles are obviously broken. To explain the above observations, when the temperature reaches 200 ℃, the rubber particles have become softened or even partially melted, so the degree of bonding with cement matrix will decrease slightly after cooling. Under 400 ℃, parts of the rubber particles begin to vaporize, and the escape of gas will produce pores in the concrete structure. Under 600 ℃ and 800 ℃, more pores will be produced in the concrete structure, ultimately resulting in the phenomenon shown in Fig. 6. A more detailed analysis can be found in the later section.

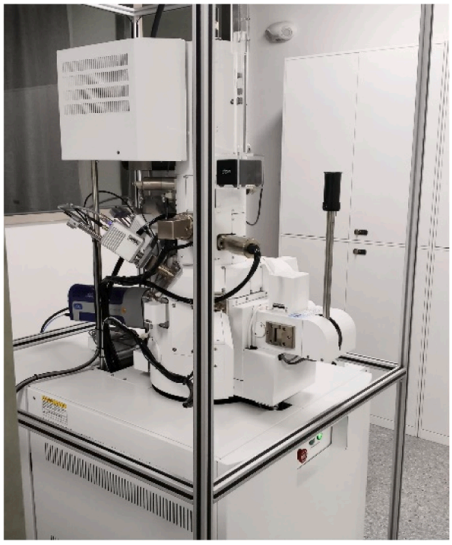

Fig. 4. SEM device.

3.2. P-CMOD curve

From the results of fracture tests on RC considering different rubber replacement rates after high-temperature treatment, the average *P*-CMOD curves were obtained, as shown in Fig. 7. All the *P*-CMOD curves exhibit similar evolution trends with either the increase of temperature or rubber replacement rate. Based on the potential failure mechanism of concrete materials, these curves can be divided into three stages, including stage I: linear elastic stage; stage II: stable expansion stage; stage III: unstable expansion stage.

According to Fig. 7, during stage I, i.e., the initial loading stage, the *P* value is at a relatively low level, not sufficient to cause the propagation of prefabricated crack. The specimen as a whole is in the elastic stage, and *P* is linearly correlated with CMOD. Throughout this stage, the specimen accumulates energy continuously. When the CMOD reaches the critical value, the accumulated energy begins to release gradually, and the prefabricated crack begins to develop. At this moment, the specimens enter stage II. The loss of energy will reduce the load slightly, manifested as the deacceleration of the growth rate of *P* as CMOD increases. After reaching the peak load, the specimens enter stage III, and the crack propagation speed begins to accelerate. Meanwhile, the internal microcracks quickly converge towards the propagation path of the prefabricated crack, and the bearing capacity of the specimen rapidly decreases. Besides, the macro-crack quickly emerges and penetrates the whole specimen.

In terms of the evolution trend of the *P*-CMOD curve, when the temperature remains constant, the *P*-CMOD curves of RC specimens exhibit similar patterns compared to that of PC. However, as the rubber replacement rate increases, the peak load value shows a decreasing trend while the CMOD value shows an increasing trend. When the rubber replacement rate remains constant, as the temperature rises, the peak load value of RC specimens significantly decreases, while the CMOD value shows a gradually increasing trend. Accordingly, the proportion of stage II, i.e., the plastic stage, increases, whereas the

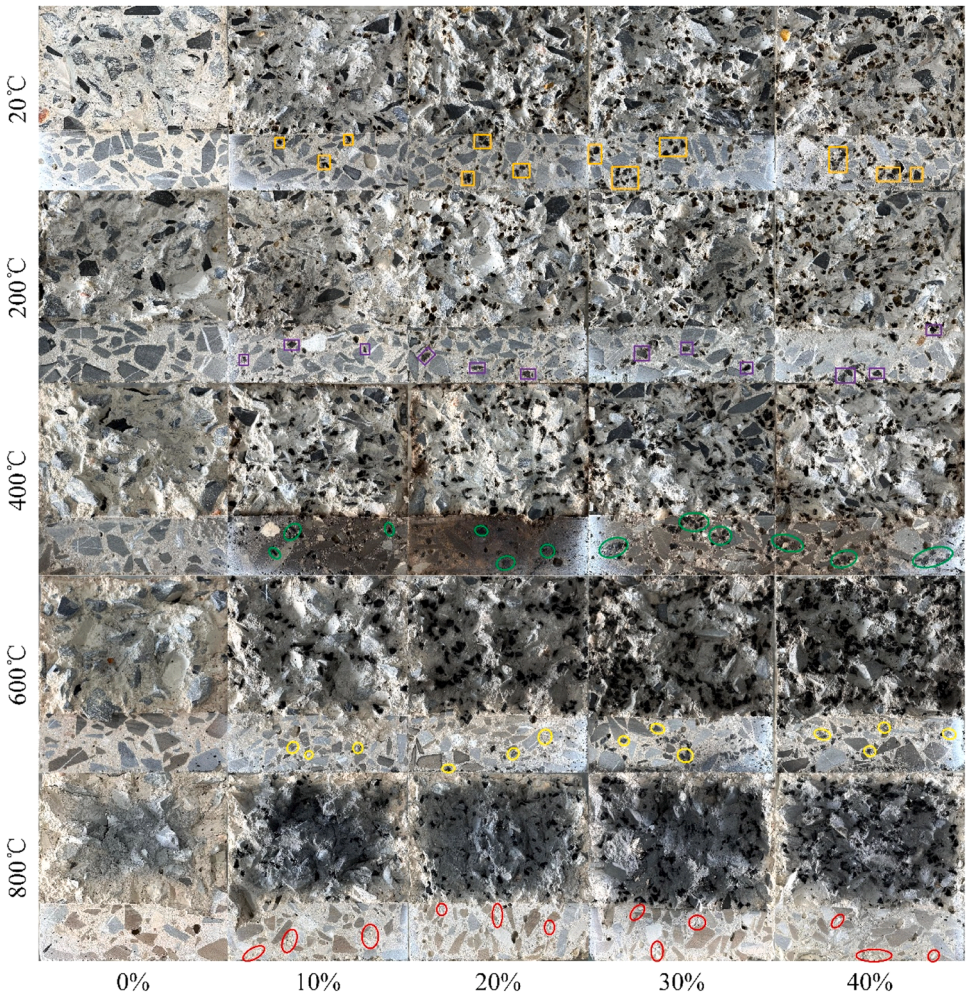

Fig. 5. Failure morphology of RC specimens under different test conditions.

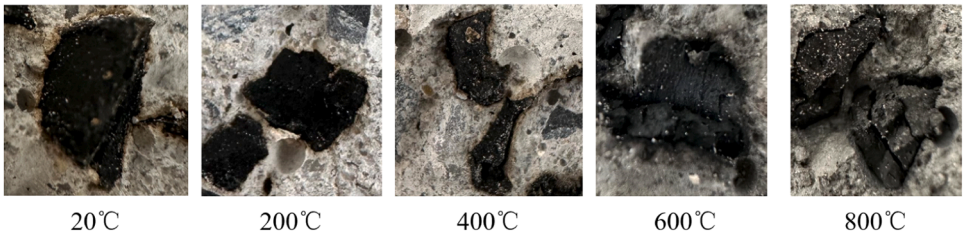

Fig. 6. Effects of temperature on the interface between rubber particles and cement matrix.

proportion of the elastic stage decreases correspondingly.

3.3. Peak load and CMOD

Further, the peak load (i.e. P_{un}) and the corresponding CMOD values were extracted from the *P*-CMOD curves to clarify the effects of temperature and rubber replacement rate on the fracture properties of concrete, as shown in Fig. 8. According to the overall trend analysis, it can be seen that as the temperature or rubber replacement rate increases, the *P* value of RC specimens gradually decreases, while the CMOD value gradually increases. Taking 40 % rubber replacement rate as an example, the growth rates of *P* and CMOD relative to PC are indicated in Fig. 8. When the temperature does not exceed 400 ℃, the weakening effect of rubber particles on the *P* value does not change significantly with the rise of temperature, but the strengthening effect on the CMOD value is slightly increased. Under 600 ℃ and 800 ℃ treatments, the weakening effect of rubber particles on the *P* value is significantly intensified, while the strengthening effect on the CMOD value is significantly reduced. Below explains how the above trend happens. For PC, the free water and bound water inside the specimen will evaporate at 200 ℃, which increases the pore size and leads to the formation of internal initial defects. At 400 °C and 600 °C, the hydration products $Ca(OH)_2$ and C-S-H gel begin to decompose, leading to a decrease in the strength of cement matrix. At 600 °C and 800 °C, the C-S-H gel decomposes sharply, and some components in the aggregates will undergo crystal transformation, leading to volume expansion. However, the thermal expansion coefficient varies between the cement matrix and coarse aggregates, resulting in further expansion of internal defects and reduction of the matrix strength. On the other hand, these defects will enhance the overall plasticity of the specimen, so that the CMOD value

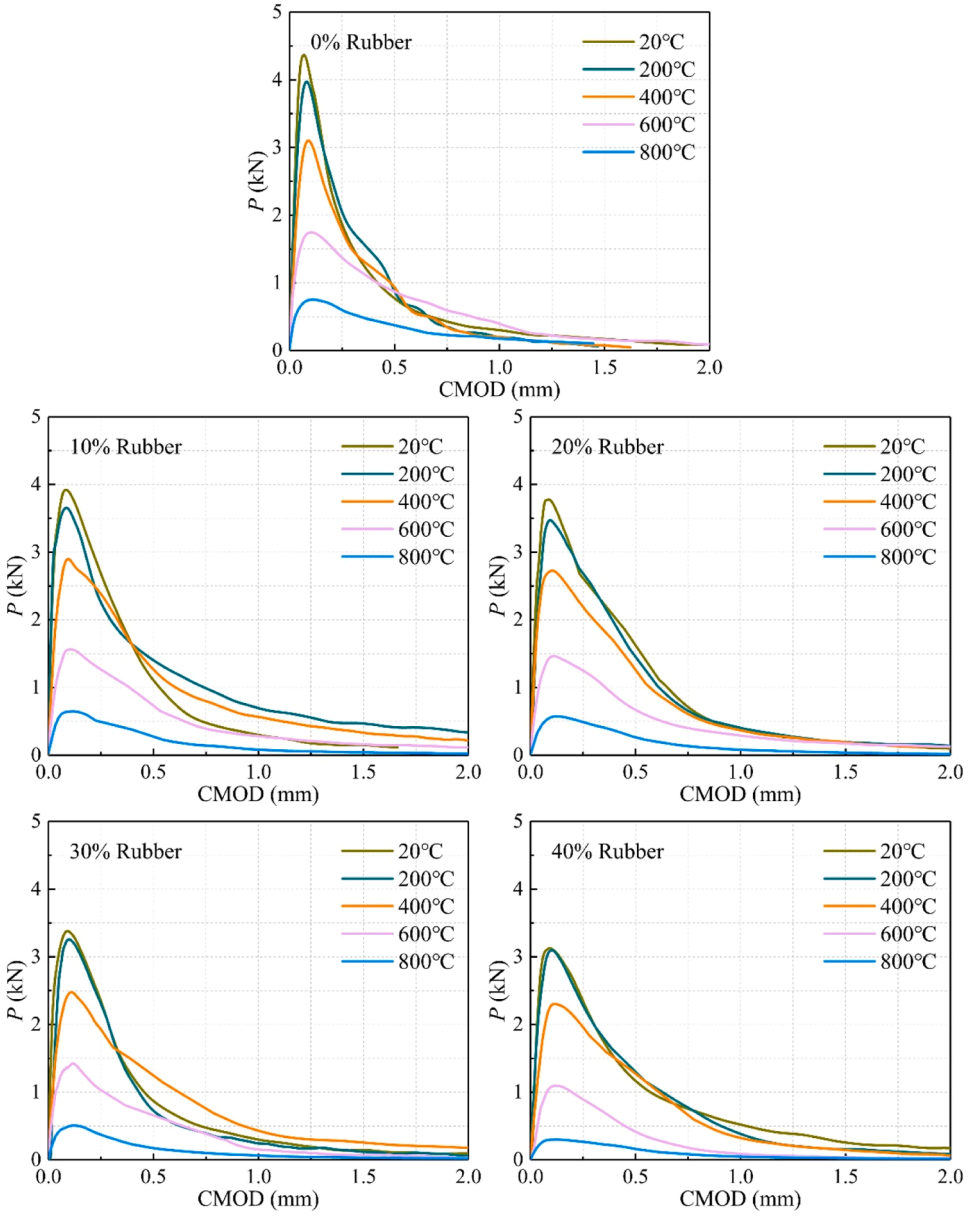

Fig. 7. *P*-CMOD curves of RC specimens.

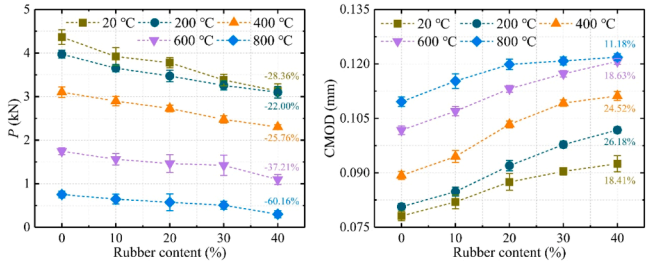

Fig. 8. Peak load and the corresponding CMOD.

corresponding to the peak load is increased [30]. For RC specimens, rubber particles will gradually undergo the softening, melting, and vaporization processes as the temperature rises. Upon the softening process, the rubber particles can serve as a soft filling material to promote the redistribution of internal stress caused by elevated temperature [4]. The melting process will produce pores between rubber particles and the matrix, resulting in a significant decrease in bearing capacity. The vaporization process will form microcracks and pores around the rubber particles, which significantly reduces the bearing capacity. As a flexible filler material, although rubber particles may reduce the strength of concrete, but will affect crack propagation so as to improve the brittleness of concrete [31], manifested as an increase in CMOD. Based on the characteristics of rubber particles mentioned above, when the temperature remains constant and does not exceed 400 ℃, the rubber particles are mainly in a softened and partially melted state. Therefore, as the rubber replacement rate increases, the strength of the specimen shows a decreasing trend while the CMOD showing an opposite trend. When the temperature reaches 600 ℃ and 800 ℃, the rubber particles are in the vaporization stage. As the rubber replacement rate increases, the deterioration effect caused by vaporization becomes stronger, manifested as a greater loss of strength and a reduced increase magnitude in CMOD.

3.4. Fracture parameters

The double-K fracture criterion is often used to obtain the initiation toughness K_{IC}^{ini} and the unstable toughness K_{IC}^{un} of materials, thereby facilitating a quantitative analysis of the initiation and propagation of cracks [32–34]. The initial cracking load P_{ini} was calculated using the curve method, which has similar precision as the strain gauge method [33]. The curve method defines the endpoint of the linear segment in *P*-CMOD curve as P_{ini}. The corresponding K_{IC}^{ini} was calculated using Eqs. (1) and (2) below:

$$K_{IC}^{ini} = \frac{3P_{ini}S}{2h^2B}\sqrt{a_0}F\left(\frac{a_0}{h}\right) \tag{1}$$

$$F\left(\frac{a_0}{h}\right) = \frac{1.99 - (a_0/h)(1-a_0/h)\left[2.15 - 3.93a_0\Big/h + 2.7(a_0/h)^2\right]}{(1+2a_0/h)(1-a_0/h)^{\frac{2}{3}}} \tag{2}$$

Where, P_{ini} is the initial cracking load, kN; S is the span length of the beam, mm; B is the width of the beam, mm; h is the height of the beam, mm; a_0 is the prefabricated crack height, mm.

To calculate K_{IC}^{un}, a_0 in Eq. (1) should be replaced with the equivalent crack critical length a_c, and the initial cracking load should be replaced with the peak load. Based on the assumption of linear asymptotic superposition [32], a_c and the equivalent elastic modulus E can be obtained using Eqs. (3) and (4) as follows:

$$a_c = \frac{2}{\pi}(h+h_0)\arctan\left(\frac{BEV_c}{32.6P_{un}} - 0.1135\right)^{\frac{1}{2}} - h_0 \tag{3}$$

$$E = \frac{1}{BC_e}\left[3.7 + 32.6\tan^2\left(\frac{\pi}{2}\frac{a_0+h_0}{h+h_0}\right)\right] \tag{4}$$

Where, h_0 refers to crack width, mm; V_c refers to crack opening displacement at P_{un}, mm; P_{un} refers to peak load, kN; C_e refers to initial flexibility.

The fracture energy G_f can be calculated by Eq. (5).

$$G_f = \frac{W_0 + mg\delta_c}{A_{lig}} \tag{5}$$

Where, W_0 refers to external work; m refers to beam mass, kg; δ_c refers to

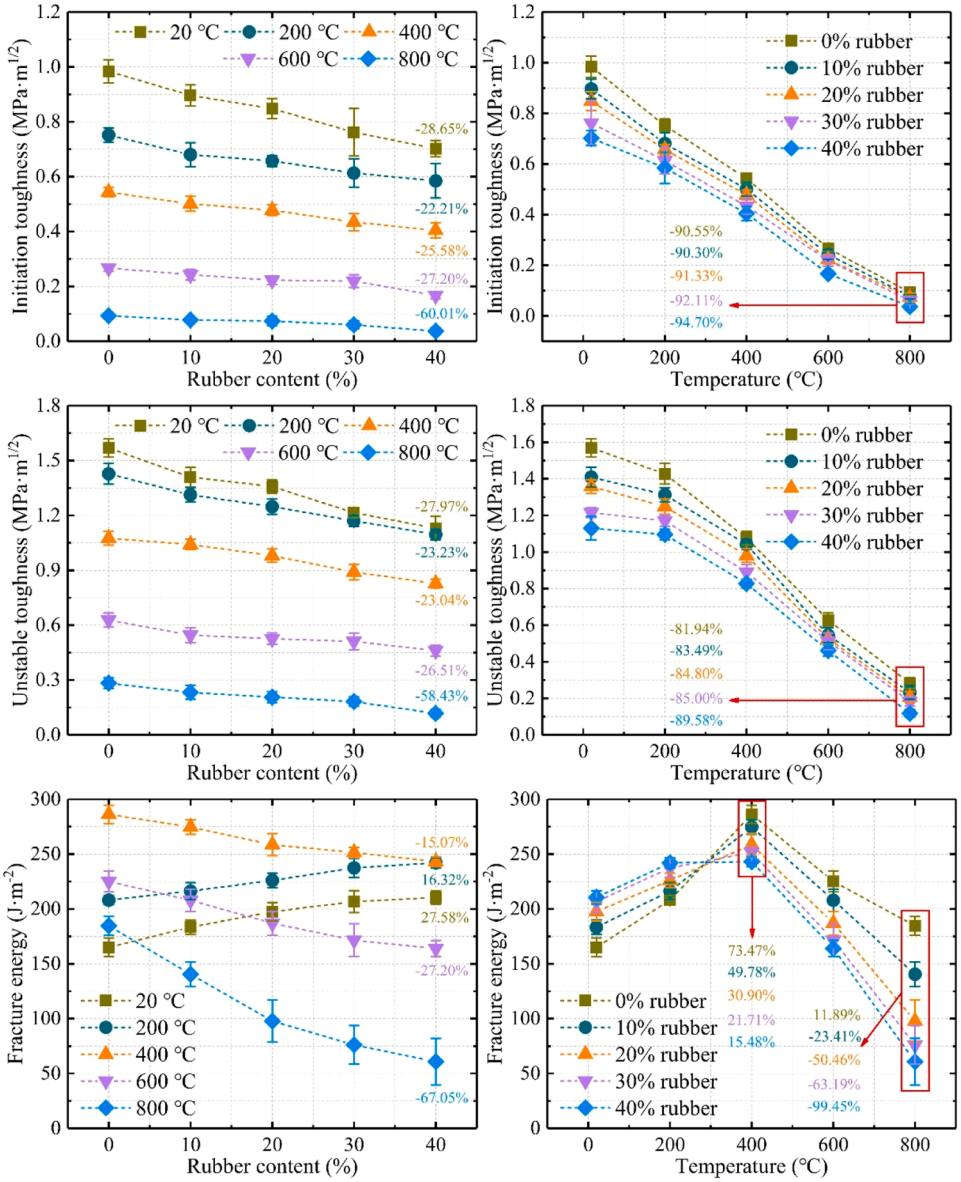

Fig. 9. Double-K fracture parameters and fracture energy.

final deformation in the mid span, mm; g is equal to 9.8 m/s^2; A_{lig} is the area of fractured ligament, mm^2.

Based on Fig. 7 and above Equations, the fracture characteristic parameters K_{IC}^{ini}, K_{IC}^{un} and G_f were calculated, as shown in Fig. 9.

According to Fig. 9, when the temperature remains constant, both K_{IC}^{ini} and K_{IC}^{un} exhibit a decreasing trend with the increase of rubber replacement rate. After 800 ℃ treatment, the rubber replacement rate has the most significant effects on the decrease magnitude of K_{IC}^{ini} and K_{IC}^{un} (decreased by 60.01 % and 58.43 %, respectively). When the rubber preplacement rate remains constant, both K_{IC}^{ini} and K_{IC}^{un} exhibit a significant decreasing trend with the rise of temperature. From the overall trend analysis, it can be seen that with the increase of rubber replacement rate, the decrease magnitude of K_{IC}^{ini} and K_{IC}^{un} shows an increasing trend with the rise of temperature, and reaches the peak level at 800 ℃ (decreased by 94.70 % and 89.58 %, respectively). The influence of rubber particles on the G_f of RC varies significantly under different temperature treatments. When the temperature is below 400 ℃, G_f shows an increasing trend with the increase of rubber replacement rate; when the temperature reaches 400 ℃ or above, G_f turns to a decreasing trend with the increase of rubber replacement rate. Moreover, when the rubber replacement rate remains constant, G_f shows a trend of first increasing and then decreasing with the rise of temperature, and reaches its peak value at 400 ℃. The above phenomenon can be explained as follows. The evolution trends of K_{IC}^{ini} and K_{IC}^{un} can be explained by similar principles described in Sections 3.1–3.2. Specifically, as the temperature rises from 20 ℃ to 800 ℃, rubber particles will gradually undergo the softening, melting, and vaporization processes. Thus, the bonding performance between rubber particles and the cement matrix will gradually deteriorate, resulting in a reduction in bearing capacity. Correspondingly, P_{ini} and K_{IC}^{ini} will decrease as well. Besides, rubber particles are a flexible filler material, so the increase in rubber content will also lead to a reduction in P_{ini} and K_{IC}^{ini}. The parameter K_{IC}^{ini} describes the ability of concrete to resist cracking, while K_{IC}^{un} describes the ability of concrete to resist unstable crack propagation. The two have similar mechanisms and ultimately exhibit the evolution trends as shown in Fig. 9.

Parameter G_f describes the energy absorption capacity of concrete. When the temperature does not exceed 200 ℃, only a very small part of rubber particles will undergo physical changes, and their performance after cooling remains similar to that under 20 ℃ treatment. At this moment, rubber particles can serve as centers of deformation. When the cracks propagate to the vicinity of rubber particles, the flexibility of rubber particles can alleviate the stress concentration at the crack tip and slow down the further development of cracks. Since the cracks cannot directly break through rubber particles, they will propagate along the interfaces around rubber particles, leading to a higher degree of curvature of the cracking path. Consequently, the fracture of the specimen requires more energy consumption. Although the strength decreases, the cracking resistance of rubber particles still plays a major role, and the fracture energy of the specimen shows an upward trend with the increase of rubber replacement rate. When the temperature reaches 400 ℃ or above, due to the gradual melting and vaporization of rubber, the interfacial performance between rubber particles and the cement matrix will severely deteriorate, resulting in a reduction in the energy required for crack propagation (i.e., the fracture energy is reduced). Moreover, as the temperature rises, crack propagation becomes easier, and the corresponding decrease magnitude in fracture energy is increased, ultimately presenting the evolution trend as shown in Fig. 9.

In order to further analyze the data dependence between fracture parameters and test variables, Fig. 10 shows the growth rates of K_{IC}^{ini}, K_{IC}^{un} and G_f for different rubber contents or temperatures. The data used in Fig. 10 are from the data set analyzed in Fig. 9, with error bars indicating standard deviation. According to Fig. 10, both an increase in rubber dosage and an increase in temperature will lead to a continuous decrease in K_{IC}^{ini} and K_{IC}^{un}. It is noteworthy that the temperature-induced decrease is more significant within the scope of this study. The increase in G_f with temperature shows a trend of first increasing and then decreasing, and reaches a maximum at 400 °C. The increase in rubber dosage further exacerbates this enhancement or weakening effect. The regression

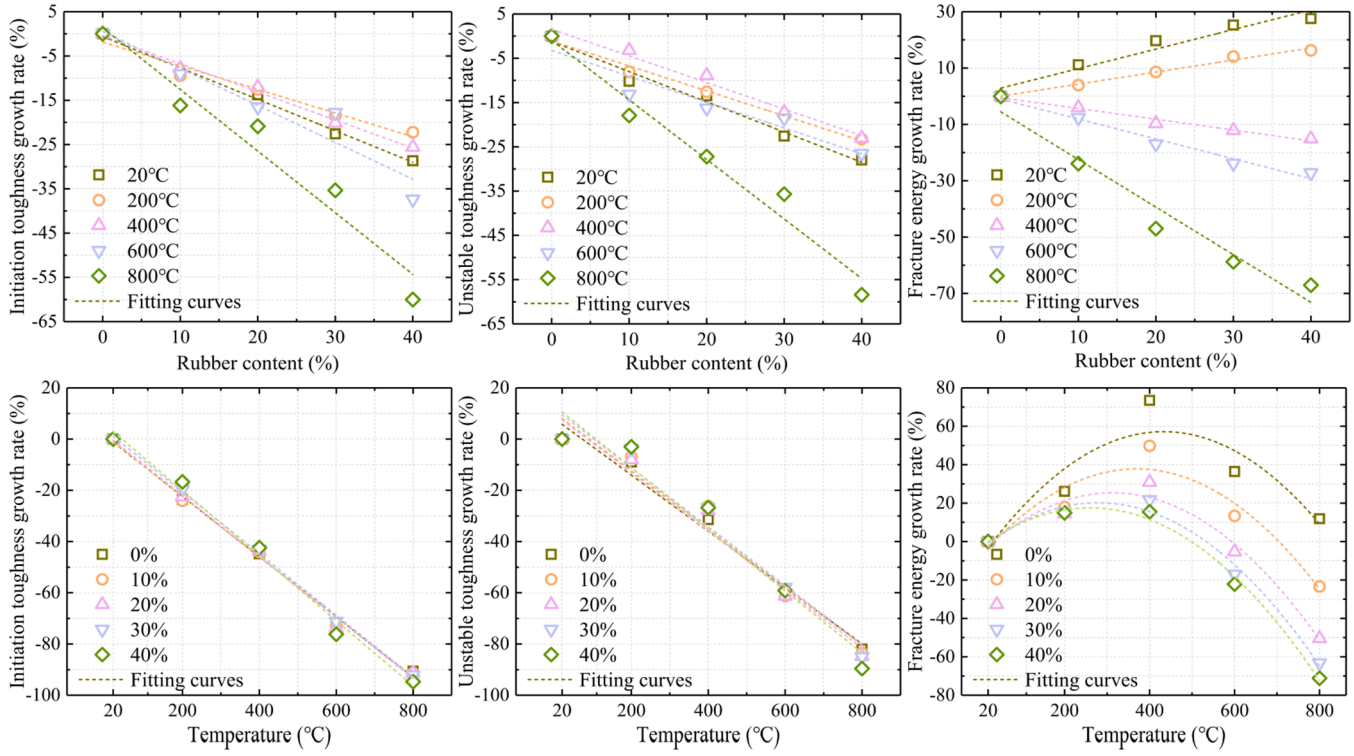

Fig. 10. Growth rates of K_{IC}^{ini}, K_{IC}^{un} and G_f with rubber content or temperature change.

curves in Fig. 10 illustrate the relationship between the growth rate of RC specimens K_{IC}^{ini}, $K_{IC}^{un}$and G_f with temperature and rubber content. Based on a phenomenological approach, the fracture energy-temperature relationship follows the equation $y = ax^2+bx+c$, while the other curves follow the equation $y = ax+b$. The specific results are enumerated in Tables 4 and 5. According to the findings in Table 4, an increase in temperature leads to a transition in the relationship between RC's G_f and rubber content, shifting from a positive correlation to a negative one. Additionally, K_{IC}^{ini} and K_{IC}^{un} demonstrate a consistent negative correlation, though their sensitivity increases with rising temperature. As demonstrated in Table 5, the G_f of RC is a quadratic function of temperature, while K_{IC}^{ini} and K_{IC}^{un} are linear functions of temperature. It is noteworthy that the relationship between K_{IC}^{ini} and K_{IC}^{un} and temperature is less affected by the amount of rubber produced. In summary, an increase in temperature or rubber content will weaken K_{IC}^{ini} and K_{IC}^{un} of the RC specimen, while there is an optimal value for G_f. It is also noteworthy that the effect of temperature on the fracture properties of RC is more significant than that of rubber content. These findings are instrumental in facilitating the engineering application of RC. For instance, when conducting finite element simulations, the effect of temperature can be prioritized during the optimization of model parameters. Furthermore, different mathematical models can be formulated to elucidate the relationship between G_f, K_{IC}^{ini}, K_{IC}^{un} and rubber content, based on the conclusions of this study.

The preceding analysis of Fig. 9, when considered in conjunction with the statistical analysis presented herein, indicates that the fracture properties of RC are influenced by both the rubber content and the temperature. However, the temperature emerges as the primary concern, given its pivotal role in distinguishing RC from conventional concrete. The presence of rubber, a material that undergoes substantial changes in properties such as melting and vaporization at varying temperatures, underscores the significance of temperature in this context. These phenomena are expected to induce alterations in the mechanical properties and crack propagation mode of RC, as outlined in the subsequent section of this paper dedicated to mechanism analysis. Ultimately, these changes are anticipated to be reflected in the fracture properties of RC. It is noteworthy that some scholars have previously investigated the impact of temperature on the fracture properties of concrete. Their findings, as reported in [15], indicate that the fracture properties of PC and HPC exhibit a comparable temperature-dependent behavior to that observed in this study, with both K_{IC}^{ini} and K_{IC}^{un} demonstrating a downward trend. The overall crack initiation toughness of PC and HPC is lower than that of RC, while the difference in unstable toughness is not significant. G_f first increases and then decreases, reaching a maximum at 400 ℃. The maximum fracture values of PC, HPC, and RC are 18.96 %, 35.99 %, and 49.78 %, respectively. This suggests that when the rubber content is set at 10 %, the fracture performance of RC will surpass that of PC and HPC. In the context of concrete mixed with fibers, Yao et al. [35] observed that the fracture properties of concrete mixed with polypropylene fibers do not exhibit a discernible pattern with increasing temperature, and the results are highly dispersed. In contrast, the present study demonstrates that the fracture properties of RC exhibit a substantial change pattern with increasing temperature or rubber content, including a monotonic decrease and an initial increase followed by a decrease. This is advantageous for predicting and controlling the properties during engineering applications.

3.5. The analysis of damage evolution and mechanism

To clarify the initiation and evolution trends of cracks during the fracture process of RC, the image data obtained by the high-speed camera during fracture failure was further processed using the DIC technology. Given the focus of this study on Type-I fracture, only the exx strain cloud maps are analyzed, as shown in Fig. 11. To monitor the progression of the fracture, the DIC calculation area was set as a rectangular area of 40 mm× 65 mm, centered above the prefabricated crack. Taking into account the rapid evolution of cracks after high-temperature treatment and space limitation, four typical test conditions (RC0–20, RC0–800, RC40–20, RC40–800) and five typical loading stages (pre-60 %, pre-80 %, peak, post-80, post-60 %) were selected for detailed analysis. In this paper, "pre-X%" refers to the stage before peak load with a load of X% of the peak value; "peak" refers to the loading stage corresponding to the peak load; "post-Y%" refers to the stage after peak load with a load of Y% of the peak value. Due to the large variation in the range of exx values among different test conditions and among different loading stages of the same test condition, each strain field cloud map was given a separate color scale.

It can be seen from Fig. 11 that the cracks in all specimens initiate from the center area (around the prefabricated crack). During the propagation process, the cracks will encounter obstacles from the cement matrix and aggregates; thus, as the loading progresses, the cracks will develop upwards and eventually form a narrow strip-shaped crack zone along the loading direction. In the PC specimen under 20 ℃ treatment (i.e., RC0–20), there are only minor cracks before the peak load, but the cracks will rapidly propagate and lose their bearing capacity after the peak load, exhibiting significant brittle failure characteristics. This evolution trend has been confirmed by the relevant literature [15,27]. Compared to RC0–20, the cracks in RC40–20 propagate even slower before the peak load. Then, during the post-peak stage, the crack propagation path tends to branch, and becomes more tortuous and complex. This is because rubber particles, as a flexible filler material, can not only effectively alleviate the stress concentration at the crack tip, thereby delaying the cracking process, but also serve as centers of local deformation. When reaching the vicinity of rubber particles, the cracks will bypass rubber particles to create more cracking paths and make the paths more tortuous and prone to branching. For the effects of elevated temperature treatment, it can be found that the occurrence of cracks in RC0–800 is significantly ahead of that in RC0–20. This is because the expansion of aggregates and cement matrix during high-temperature treatment will introduce a large number of initial defects, and high-temperature treatment will also decompose C-S-H gel and $Ca(OH)_2$, which reduces the strength and cracking resistance of concrete. This provides favorable conditions for crack initiation and propagation [3]. In addition, the crack occurrence time of RC40–800 is significantly ahead of RC0–800. This is because rubber particles will gradually undergo expansion, melting and vaporization under elevated temperature, which will cause damage to the interface layers between rubber particles and the cement matrix, resulting in a significant

Table 4
Coefficient of regression curve (rubber content).

Temperature (°C)	G_f			K_{IC}^{ini}			K_{IC}^{un}		
	a	*b*	R^2	*a*	*b*	R^2	*a*	*b*	R^2
20	0.693	2.893	0.94	−0.710	−0.596	0.99	−0.683	−1.178	0.98
200	0.428	0.037	0.99	−0.534	−1.859	0.97	−0.564	−1.078	0.99
400	−0.382	−0.525	0.98	−0.635	−0.409	0.99	−0.601	1.559	0.98
600	−0.705	−1.019	0.98	−0.835	0.546	0.91	−0.584	−3.209	0.91
800	−1.690	−5.552	0.95	−1.392	1.358	0.95	−1.346	−0.923	0.97

Table 5
Coefficient of regression curve (temperature).

Rubber content (%)	G_f				K_{IC}^{ini}			K_{IC}^{un}		
	a	*b*	*c*	R^2	*a*	*b*	R^2	*a*	*b*	R^2
0	−3.6E−04	0.308	−9.347	0.83	−0.117	1.097	1.00	−0.110	7.931	0.98
10	−3.4E−04	0.249	−8.104	0.89	−0.118	1.211	1.00	−0.113	10.276	0.96
20	−3.2E−04	0.201	−6.126	0.96	−0.119	1.946	1.00	−0.114	9.698	0.97
30	−3.1E−04	0.174	−4.047	0.98	−0.120	3.469	1.00	−0.115	11.754	0.96
40	−3.1E−04	0.159	−3.125	0.99	−0.127	5.359	0.99	−0.121	13.017	0.95

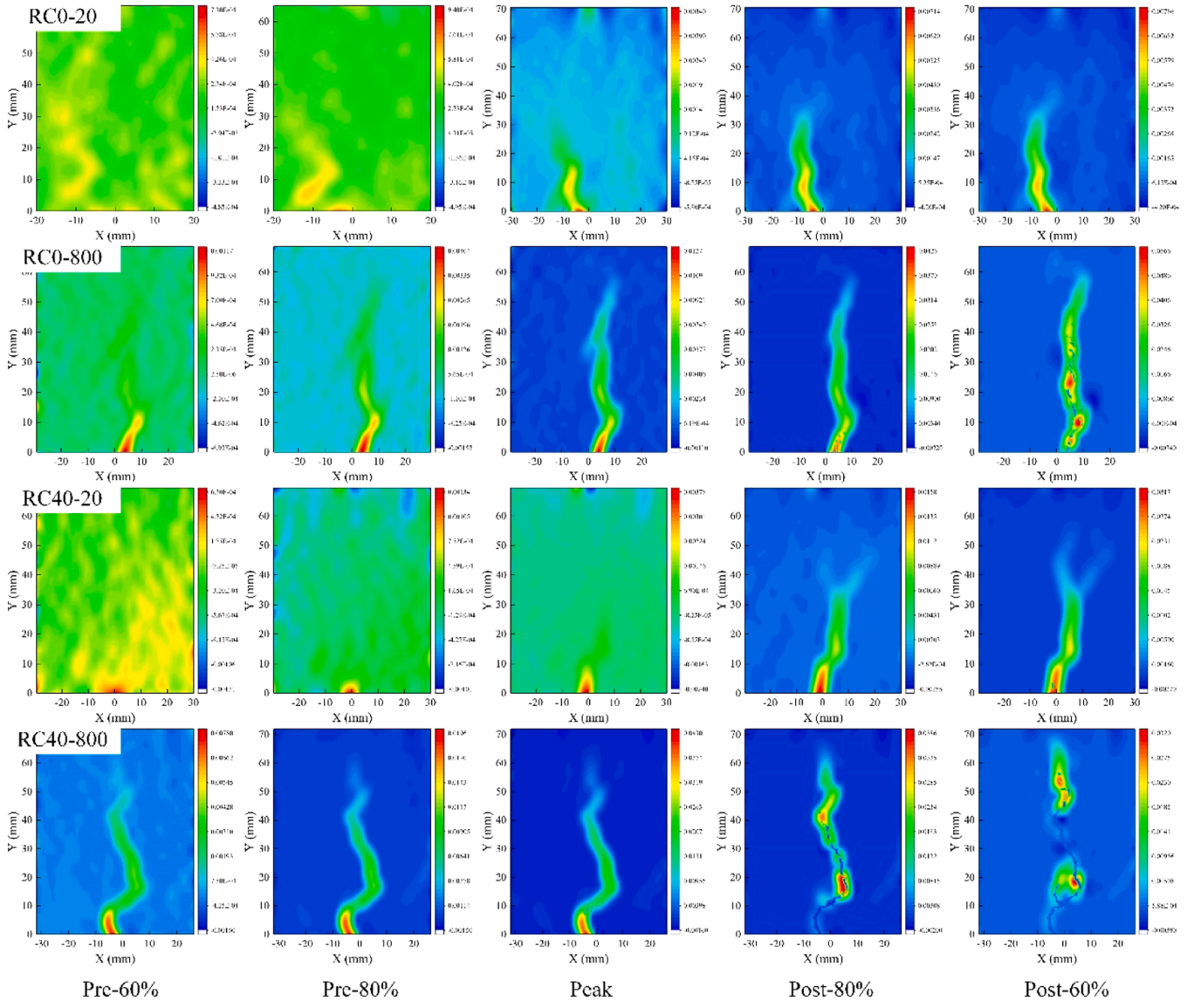

Fig. 11. Crack initiation and evolution processes of RC.

reduction in the bearing capacity and cracking resistance of concrete during the loading process. Therefore, it can be concluded that rubber particles can effectively improve the cracking resistance of concrete, but after high-temperature treatment, the performance of RC is inferior to that of PC.

To clarify the mechanism underlying the effects of rubber particles on the cracking resistance of concrete, SEM equipment was employed to analyze the interfacial performance between rubber and mortar matrix after treatments by different temperatures, and the microstructure obtained was shown in Fig. 12. According to Fig. 12, after 20 ℃ treatment, rubber particles are tightly bound to the matrix; as the temperature rises, the interface gradually deteriorates. After 200 ℃ treatment, cracks are formed at the rubber-matrix interface, and a certain degree of separation can be observed between the two. This is because with the increase of temperature, the difference in thermal expansion coefficient between rubber particles and the matrix will lead to occurrence of cracks at the interface layer during the heating and cooling processes. However, after 400 ℃ treatment, the cracks at the rubber-matrix interface are healed, which is due to the fact that rubber particles will melt under this temperature and the cracks caused by thermal expansion will be refilled and

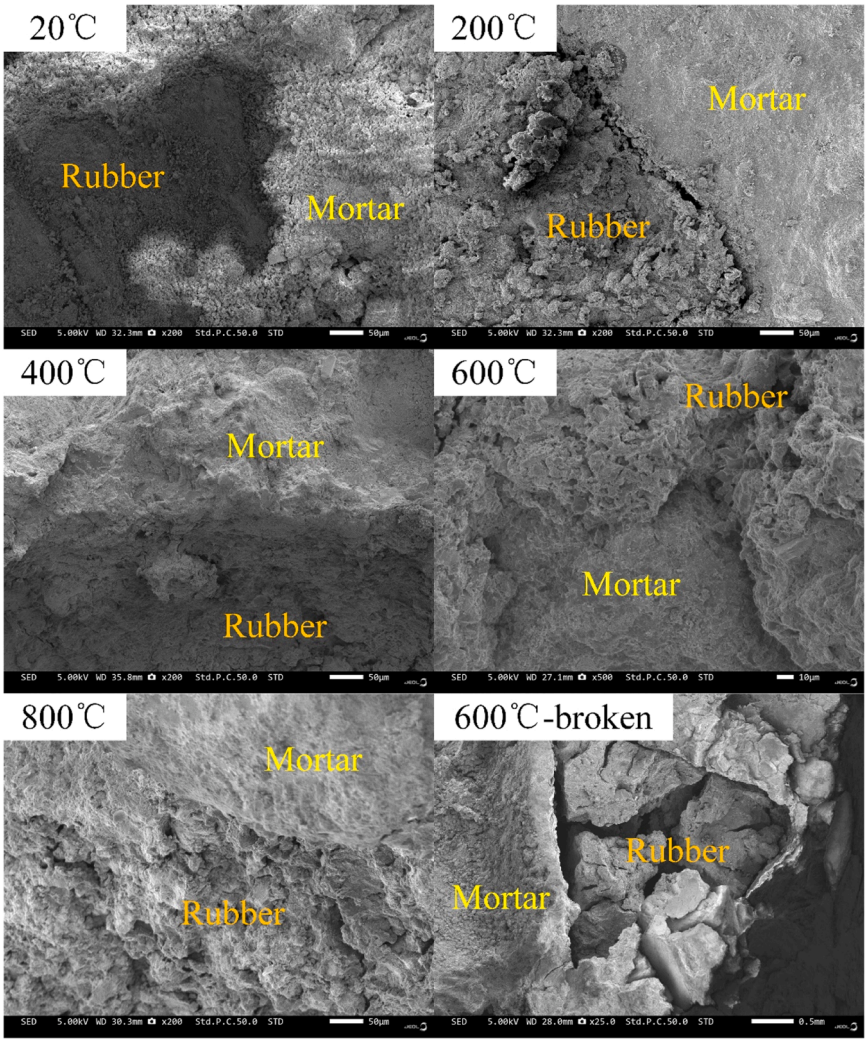

Fig. 12. Analysis of the interfacial morphology between rubber and mortar matrix.

bridged by liquid rubber. Thus, the situation shown in Fig. 12 was observed. As the temperature reaches 600 ℃, parts of the rubber particles will begin to vaporize to form pores, resulting in residual pores on the surface of rubber particles after cooling, as shown in Fig. 12. This phenomenon can be observed more obviously after 800 ℃ treatment due to a higher degree of vaporization. The formation of these pores and cracks will result in a reduction of the RC's fracture mechanical properties. It is worth noting that due to the presence of pores after the thermal expansion and contraction process, the rubber particles treated under 600 ℃ have begun to break, which further exacerbates their deteriorating effect on the fracture properties of concrete. This is also an important factor explaining why the fracture properties of the specimens corresponding to 600 ℃ and 800 ℃ treatments were significantly weakened. This provides essential guidance for the engineering application of RC. Despite the fact that rubber particles can lead to a reduction in concrete's strength, they play a crucial role in enhancing its toughness. However, when the temperature exceeds 400℃, the efficacy of rubber particles must be reevaluated by engineers.

To verify the changes of rubber particles at different temperatures, the backscattered electron-energy dispersive spectroscopy (BSE-EDS) technique was employed to obtain information on the elemental changes of rubber particles at different temperatures, as shown in Fig. 13. Rubber and cement hydration products are represented by the elements C and Ca, respectively. According to the elemental information, a small amount of cement hydration products are scattered on the surface of the rubber particles.As the temperature increases, these hydration products gradually decompose, and their volume also decreases (if they are attached to cement hydration products).According to the change in the distribution of the C element, there is no significant change in the elemental density of the rubber at different temperatures, i.e., no significant chemical reaction has occurred. The BSE and EDS results indicate that as the temperature rises to 400 ℃, the surface roughness of the rubber gradually decreases, suggesting that the micro-protrusions on the surface gradually dissolve under the influence of temperature and maintain a flat state after cooling. However, at temperatures of 600 ℃ and 800 ℃, there was a substantial increase in the roughness of the rubber surface. This can be attributed to the fact that the high temperature not only melted the rubber but also caused partial vaporization, resulting in a fluctuating state of liquid rubber. Upon cooling, the surface lost its flatness, and it was evident that numerous holes remained. Furthermore, at temperatures of 600 ℃, the rubber exhibited a tendency to fragment, manifesting as cracks on the surface. These observations serve to substantiate the aforementioned hypothesis concerning the mechanism of action of rubber.

According to the previously mentioned mechanism of RC crack propagation, a model of the mechanism of RC crack initiation and evolution can be obtained, with a same time (see Fig. 14). For the PC specimen at room temperature, the crack originates from the center and continues to expand along the main direction of stress, exhibiting twists and turns under the influence of coarse aggregates. The incorporation of

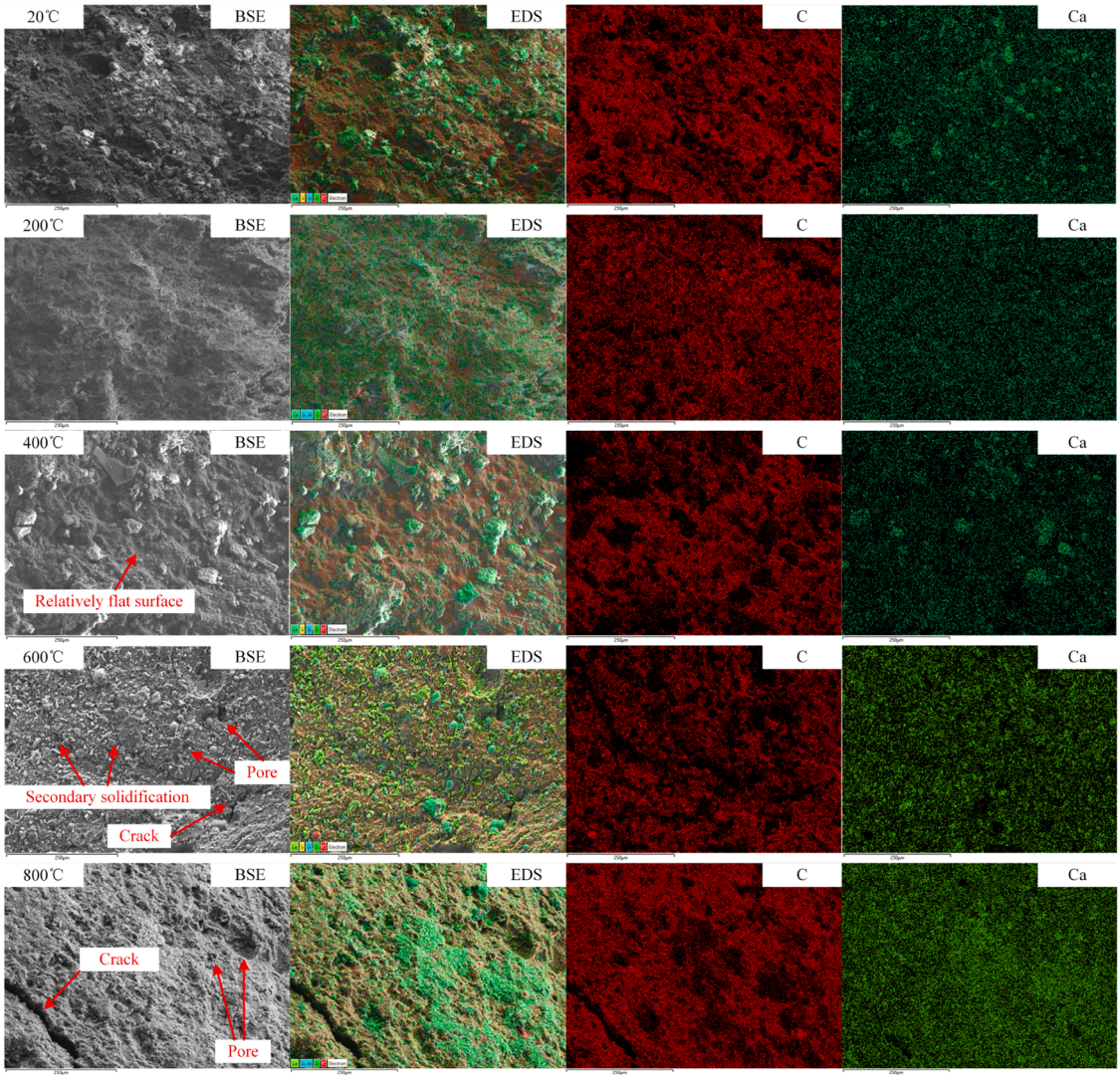

Fig. 13. BSE-EDS results of rubber particles at different temperatures.

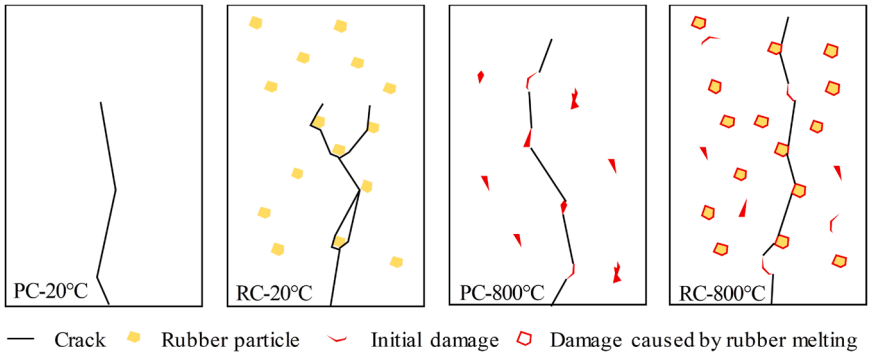

Fig. 14. Mechanism model of RC crack initiation and evolution.

rubber particles serves to mitigate the phenomenon of stress concentration, thereby hindering the formation of new branches of the crack near the rubber, as depicted in Fig. 14. With an increase in temperature, specifically at 800 ℃, the expansion of the aggregate and rubber within the matrix gives rise to a substantial number of initial defects. These defects, in turn, expedite the progression of the crack through the PC specimen, culminating in the formation of a single, primary crack. For the RC specimen, a significant number of defects are also introduced by the rubber melting process, resulting in a crack development pattern analogous to that of the PC specimen, albeit at an accelerated rate. The higher incidence of initial defects arising from rubber melting and vaporization, in comparison to other methods, coupled with the significant escalation in defect formation that accompanies an increase in rubber content, renders the temperature effect of the aforementioned crack propagation mode more pronounced. This results in the manifestation of cracks that are more linear and rapid. The proposed model of

crack evolution mechanism offers a mechanistic framework and insights that can inform the advancement of RC methodologies.

3.6. The process of crack propagation

Crack tip opening displacement (CTOD) is an effective parameter to study the process of unstable crack propagation [27,29]. CTOD measures the distribution characteristics of cracks by analyzing the sudden changes in horizontal displacement at different horizontal positions. In this paper, a series of parallel horizontal acquisition lines with a spacing of 5 were set in the horizontal displacement cloud map for the purpose of extracting the corresponding horizontal displacement of each point on the lines. The amplitude of the horizontal displacement jump was taken as the CTOD value (see Fig. 15 for the specific calculation method). A total of 7 loading stages (pre-40 %, Pre-60 %, pre-80 %, peak, post-80 %, post-60 %, pre-40 %) were selected to analyze the evolution pattern of CTOD, and the results are shown in Fig. 16.

According to Fig. 16, as the value of y increases, the CTOD values of all specimens exhibit a decreasing trend, which is consistent with the crack characteristics shown in Fig. 11. From the CTOD values at different loading stages, it can be found that the addition of rubber particles can effectively increase the CTOD value. This is because rubber particles can serve as deformation centers during the cracking process, therefore alleviating the problem of rapid failure caused by stress concentration and prolonging the crack propagation path. This can improve the cracking resistance of concrete while delaying the crack propagation speed; as a result, the specimen can withstand greater deformation. For PC specimens, the CTOD of RC0–800 is significantly higher than that of RC0–20. This is because elevated temperature can cause decomposition of the cement matrix and aggregates, leading to concrete degradation. After adding rubber particles, the melting and vaporization of rubber particles under high-temperature treatment will produce more initial defects in RC specimens than in PC, leading to further deterioration of concrete. It is worth noting that at room temperature, the CTOD of RC0–20 shows a more tortuous evolution pattern with the increase of the value of y compared to RC40–20. This is because the addition of rubber particles alleviates the stress concentration at the crack tip during the cracking process, and the weak interfaces around rubber particles provide more low-energy path options for crack propagation. As a result, the cracks do not have to accumulate energy continuously in order to pass through the cement matrix that requires high energy consumption. Due to the need for further propagation at the crack tip, the cracks need to accumulate enough energy at the tip area so as to penetrate the cement matrix for further propagation. Therefore, considering that different parts of the matrix require different energy for cracking, the difficulty of cracking varies across the cement matrix, resulting in inconsistent opening displacements. When rubber particles are added, the presence of rubber particles can help cracks penetrate through weaker areas in the matrix with similar energy consumption.

For concrete materials, fracture process zone (FPZ) is also a parameter that is often used to describe crack propagation in the relevant literature [21,27], especially using the distance from the crack tip to the crack bottom, i.e., the FPZ length, to describe the degree of material failure. In general, positions with CTOD values less than 5 μm are considered as crack tips for the purpose of determining the FPZ length [27]. Therefore, based on the CTOD values shown in Fig. 16, the FPZ lengths corresponding to specimens under different test conditions were obtained, as shown in Fig. 17. Overall, the FPZ length increases tortuously during the loading process, and the degree of tortuosity depends on the heterogeneity of the concrete material. Meanwhile, the growth rate of the FPZ length shows a trend of first increasing and then decreasing as the loading progresses. As mentioned in the CTOD analysis section, rubber particles can help cracks quickly locate more easily cracked areas. Therefore, under the same temperature, the FPZ of RC specimens appears earlier than that of PC. At room temperature, although the appearance of FPZ in RC0–20 lags behind RC40–20, the FPZ length of RC0–20 develops to its peak value at a faster rate. This is because rubber particles can cause the crack propagation path to grow, while slowing down the crack propagation speed. After 800 ℃ treatment, as a large number of initial detects are produced, there are more positions for crack initiation in the specimen, making crack initiation easier; as a result, the FPZ appears earlier compared to 20 ℃ situation. Due to the severe degradation of RC specimens by elevated temperature treatment, the FPZ of RC40–800 has already appeared and developed to a certain length in the pre-40 % stage. In summary, under temperatures that are not high enough to vaporize rubber, the addition of rubber particles may lead to an earlier initiation of cracks in concrete, but it can significantly delay the propagation of cracks, providing better cracking resistance to concrete materials. This finding indicates that the incorporation of rubber particles in engineering can modify the mode of crack propagation. Furthermore, RC has been demonstrated to effectively delay the complete failure of structures that permit a certain degree of cracking in concrete.

4. Conclusions

In this study, three-point bending fracture tests were carried out on RC specimens with different rubber replacement rates (0 %, 10 %, 20 %, and 30 %) under different treatment temperatures (20 ℃, 200 ℃, 400 ℃, 600 ℃, and 800 ℃). Then, the effects of rubber replacement rate and temperature on the fracture properties of concrete as well as the underlying mechanism were analyzed by employing the DIC and SEM

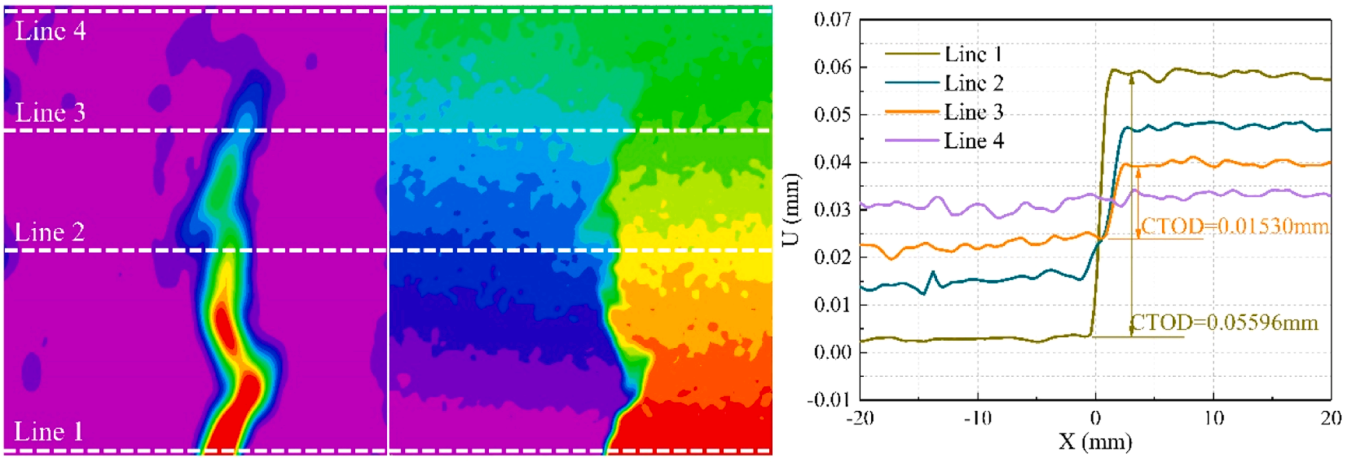

Fig. 15. Illustration of the CTOD calculation principle.

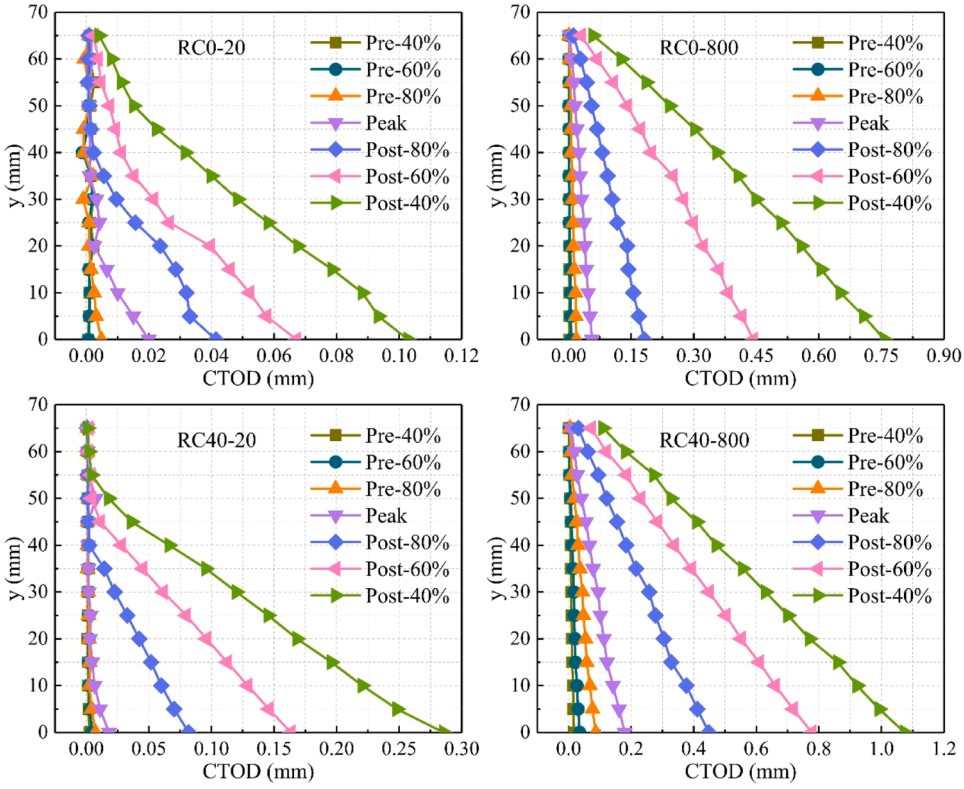

Fig. 16. CTOD of RC specimens.

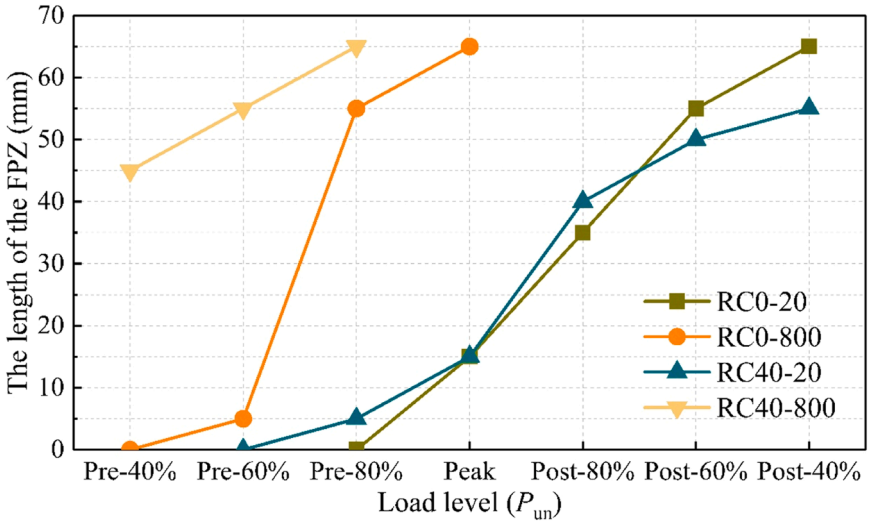

Fig. 17. Variation trend of the FPZ length in RC specimens.

technology. The main conclusions are summarized as follows:

(1) The addition of rubber particles can weaken the fracture load of concrete to a certain extent, but can enhance its toughness. Such effects are positively correlated with the rubber replacement rate. Compared to RC0–20, the growth rates of P, CMOD, K_{IC}^{ini}, K_{IC}^{un} and G_f in RC40–20 are −28.36 %, 18.41 %, −28.65 %, 27.97 %, and 27.58 %, respectively. Elevated temperature treatment can cause severe deterioration to the fracture properties of concrete, especially for concrete containing rubber particles. Compared to RC0–800, the growth rates of P, CMOD, K_{IC}^{ini}, K_{IC}^{un} and G_f in RC40–800 are −60.16 %, 11.18 %, −60.01 %, −58.43 %, and −67.05 %, respectively.

(2) For concrete specimens treated under 200 ℃ or below, rubber particles are conducive to improving the toughness of concrete, but may result in a loss of strength. For specimens treated under higher temperatures, rubber particles mainly exhibit a deteriorating effect on the overall performance of concrete due to melting and vaporization. Especially when the temperature reaches 600 ℃ and above, rubber particles will exhibit fragmentation, which may further exacerbate the deteriorating effect.

(3) As the temperature rises, the microstructure of rubber particles gradually changes from a relatively uniform state in close contact

with the cement matrix to a fragmented state filled with pores separated from the matrix. This transition will lead to severe deterioration of concrete performance. Under temperatures that are not high enough to vaporize rubber (i.e., not exceeding 400 ℃), rubber particles mainly affect the initiation and propagation of cracks by alleviating the stress concentration at the crack tip and improving the crack propagation path. More specifically, the addition of rubber particles can make the crack initiation time earlier, but significantly delay the crack propagation process.

Nevertheless, the present study concentrates predominantly on the RC fracture properties following immediate heating, and although the conclusions described herein are beneficial for the engineering application of RC, the long-term performance of building materials in engineering applications remains a pivotal factor that cannot be disregarded. The deterioration of concrete and rubber due to temperature is almost irreversible, including chemical changes in cement hydration products and changes in the physical properties of rubber and its surrounding matrix. Consequently, RC will exhibit different properties during service than traditional concrete. Conducting sufficient research on both the short-term and long-term properties of RC is, therefore, essential to the effective promotion of the engineering application of RC. The focus of future research will thus be on the evolution of the long-term properties of RC after high temperatures.

CRediT authorship contribution statement

Aydin Beyazit Bestami: Writing – review & editing, Supervision. **Pan Tanbo:** Writing – review & editing, Supervision, Resources, Methodology, Funding acquisition, Conceptualization. **Zhou Yubao:** Writing – review & editing. **Wu Liangqin:** Writing – original draft, Project administration, Funding acquisition, Formal analysis. **Zhu Zhiyong:** Visualization, Investigation, Formal analysis. **Li Renfeng:** Writing – original draft, Investigation, Formal analysis.

Declaration of Competing Interest

The authors declare that they have no known competing financial interests or personal relationships that could have appeared to influence the work reported in this paper.

Acknowledgement

This study was substantially supported by the Key Project of Science and Technology Research and Development Plan of China National Railway Group Co., Ltd. (N2023G040), National Natural Science Foundation of China (52468023), General Project of Jiangxi Natural Science Foundation (20224BAB204064), Key Project of Science and Technology Research of Jiangxi Education Department (GJJ2200607).

Data availability

Data will be made available on request.

References

[1] T.M. Pham, M. Elchalakani, H. Hao, J. Lai, S. Ameduri, T.M. Tran, Durability characteristics of lightweight rubberized concrete, Constr. Build. Mater. 224 (2019) 584–599.
[2] A.M. Marques, J.R. Correia, J. de Brito, Post-fire residual mechanical properties of concrete made with recycled rubber aggregate, Fire Saf. J. 58 (2013) 49–57.
[3] Y. Yu, Z. Jin, D. Shen, J. An, Y. Sun, N. Li, Microstructure evolution and impact resistance of crumb rubber concrete after elevated temperatures, Constr. Build. Mater. 384 (2023).
[4] A. Turatsinze, S. Bonnet, J.L. Granju, Mechanical characterisation of cement-based mortar incorporating rubber aggregates from recycled worn tyres, Build. Environ. 40 (2) (2005) 221–226.
[5] K.B. Najim, M.R. Hall, Mechanical and dynamic properties of self-compacting crumb rubber modified concrete, Constr. Build. Mater. 27 (1) (2012) 521–530.
[6] E. Ganjian, M. Khorami, A.A. Maghsoudi, Scrap-tyre-rubber replacement for aggregate and filler in concrete, Constr. Build. Mater. 23 (5) (2009) 1828–1836.
[7] Y. Li, S. Zhang, R. Wang, F. Dang, Potential use of waste tire rubber as aggregate in cement concrete – a comprehensive review, Constr. Build. Mater. 225 (2019) 1183–1201.
[8] L. Hua, F. Xiao, Y. Li, H. Huang, K. Zhao, K. Yu, C. Hettiarachchi, A potential damage mechanism of rubberized cement under freeze-thaw cycle, Constr. Build. Mater. 252 (2020).
[9] J. Xu, Z. Fu, Q. Han, G. Lacidogna, A. Carpinteri, Micro-cracking monitoring and fracture evaluation for crumb rubber concrete based on acoustic emission techniques, Struct. Health Monit. 17 (2018) 946–958.
[10] A. Gregori, C. Castoro, G. Marano, R. Greco, Strength reduction factor of concrete with recycled rubber aggregates from tires, J. Mater. Civ. Eng. 31 (2019).
[11] Y. Yu, Z. Jin, H. Zhu, H. Song, Effect of rubber particles on impact resistance of concrete at a temperature of − 20 °C, Arch. Civ. Mech. Eng. 21 (2021) 107.
[12] Y. Peng, G. Zhao, Y. Qi, Q. Zeng, In-situ assessment of the water-penetration resistance of polymer modified cement mortars by μ-XCT, SEM and EDS, Cem. Concr. Compos. 114 (2020).
[13] Z. Yu, Q. Yang, J. Zhang, et al., Research on uniaxial mechanical performance of high-performance concrete after high temperature rapid cooling and damage mechanism analysis, J. Build. Eng. 86 (2024) 108921.
[14] Z. Yu, T. Wu, X. Sun, et al., Fracture mechanical properties and failure mechanism of high-performance concrete after freeze-thaw cycles, Eng. Fract. Mech. 315 (2025) 110795.
[15] Z. Yu, X. Zhan, M. Jiao, J. Zhang, X. Yan, T. Zhang, X. Du, Study on the fracture mechanical properties of high performance concrete (HPC) with rapid cooling after high temperature, Constr. Build. Mater. 422 (2024).
[16] Z. Li, J. Xu, E. Bai, Static and dynamic mechanical properties of concrete after high temperature exposure, Mater. Sci. Eng.: A 544 (2012) 27–32.
[17] H. Akbarzadeh Bengar, A.A. Shahmansouri, N. Akkas Zangebari Sabet, K. Kabirifar, V. W.Y. Tam, Impact of elevated temperatures on the structural performance of recycled rubber concrete: experimental and mathematical modeling, Constr. Build. Mater. 255 (2020).
[18] G. Choe, G. Kim, M. Yoon, E. Hwang, J. Nam, N. Guncunski, Effect of moisture migration and water vapor pressure build-up with the heating rate on concrete spalling type, Cem. Concr. Res. 116 (2019) 1–10.
[19] W. Feng, B. Chen, F. Yang, F. Liu, L. Li, L. Jing, H. Li, Numerical study on blast responses of rubberized concrete slabs using the Karagozian and Case concrete model, J. Build. Eng. 33 (2021).
[20] J.-h Xie, Y.-c Guo, L.-s Liu, Z.-h Xie, Compressive and flexural behaviours of a new steel-fibre-reinforced recycled aggregate concrete with crumb rubber, Constr. Build. Mater. 79 (2015) 263–272.
[21] L. Xie, X. Sun, Z. Yu, H. Lian, J. Duan, F. Zhang, W. Zhao, Fracture mechanical properties and interfacial characteristics of engineered cementitious composites containing coarse aggregate, Eng. Fract. Mech. 307 (2024).
[22] H. Xie, L. Yang, J. Li, Z. Chen, F. Zhang, Y. Liu, Z. Sui, Q. Zhang, Research on mode-I fracture characteristics of basalt fiber reactive powder concrete, J. Build. Eng. 80 (2023).
[23] CNS (China National Standards), Specification for mix proportion design of ordinary concrete. JGJ 55-2011, China Architecture and Building Press, Beijing, 2011.
[24] L. Xie, X. Sun, Z. Yu, H. Lian, Study on the tensile properties of basalt fiber reinforced concrete under impact: experimental and theoretical analysis, Arch. Civ. Mech. Eng. 24 (2) (2024).
[25] Q. Ma, R. Guo, Z. Zhao, Z. Lin, K. He, Mechanical properties of concrete at high temperature—a review, Constr. Build. Mater. 93 (2015) 371–383.
[26] L. Wang, Y. Zhao, Y. Xing, Investigating high-temperature deformation evolution of concrete under sustained loading using DIC technology and a temperature-mechanical coupled damage constitutive model, Constr. Build. Mater. 324 (2022).
[27] L. Xie, X. Sun, Z. Yu, H. Lian, H. He, L. Wang, Z. Zhang, X. Xu, Effects of nano-silica on fracture properties and mechanism analysis of basalt fiber reinforced concrete, Constr. Build. Mater. 439 (2024).
[28] R. Junru, C. Huiguo, D. Ruixi, S. Tao, Behavior of combined fly ash/GBFS-based geopolymer concrete after exposed to elevated temperature, IOP Conf. Ser.: Earth Environ. Sci. 267 (3) (2019).
[29] H. Lian, X. Sun, Z. Yu, T. Yang, J. Zhang, G. Li, Z. Guan, M. Diao, Research on the fracture mechanical performance of basalt fiber nano-CaCO3 concrete based on DIC technology, Constr. Build. Mater. 329 (2022).
[30] S. Peng, Z. Yu, Q. Zhao, X. Du, X. Xie, B. Chen, Y. Zhang, Research on dynamic compressive performance and failure mechanism analysis of concrete after high temperature and rapid cooling, Materials 15 (2022) 4642.
[31] W. Shi, H. Zhu, Y. Yu, C. Luo, J. Shan, T. Wang, Case study of a SAP-CRC bridge deck in Lu-shan County, Henan, China, Structural concrete, J. FIB 22 (2021) 1523–1533.
[32] S. Xu, H.W. Reinhardt, Determination of double-K criterion for crack propagation in quasi-brittle fracture, part I: experimental investigation of crack propagation, Int. J. Fract. 98 (1999) 111–149.
[33] S. Xu, H.W. Reinhardt, Determination of double-K criterion for crack propagation in quasi-brittle fracture, Part II: analytical evaluating and practical measuring methods for three-point bending notched beams, Int. J. Fract. 98 (1999) 151–177.
[34] S. Xu, H.W. Reinhardt, Determination of double-K criterion for crack propagation in quasi-brittle fracture, Part III: compact tension specimens and wedge splitting specimens, Int. J. Fract. 98 (1999) 179–193.
[35] X. Yao, Y. Han, L. Shen, D. Zhu, Experimental study on the effect of polypropylene fiber on compressive strength and fracture properties of high-strength concrete after elevated temperatures, J. Build. Eng. 86 (2024) 108860.